A Quasi-Mechanistic Mathematical Representation for Blood Viscosity

Samuel J. Hund [1], Marina V. Kameneva [2] and James F. Antaki [1,2,*]

[1] Department of Biomedical Engineering, Carnegie Mellon University, Pittsburgh, PA 15213, USA; shund@cerebro-scope.com

[2] Department of Bioengineering, University of Pittsburgh, Pittsburgh, PA 15260, USA; kamenevamv@upmc.edu

[*] Correspondence: antaki@cmu.edu; Tel.: +1-412-268-9857

Abstract: Blood viscosity is a crucial element for any computation of flow fields in the vasculature or blood-wetted devices. Although blood is comprised of multiple elements, and its viscosity can vary widely depending on several factors, in practical applications, it is commonly assumed to be a homogeneous, Newtonian fluid with a nominal viscosity typically of 3.5 cP. Two quasi-mechanistic models for viscosity are presented here, built on the foundation of the Krieger model of suspensions, in which dependencies on shear rate, hematocrit, and plasma protein concentrations are explicitly represented. A 3-parameter Asymptotic Krieger model (AKM) exhibited excellent agreement with published Couette experiments over four decades of shear rate (0–1000 s^{-1}, root mean square (RMS) error = 0.21 cP). A 5-parameter Modified Krieger Model (MKM5) also demonstrated a very good fit to the data (RMS error = 1.74 cP). These models avoid discontinuities exhibited by previous models with respect to hematocrit and shear rate. In summary, the quasi-mechanistic, Modified-Krieger Model presented here offers a reasonable compromise in complexity to provide flexibility to account for several factors that affect viscosity in practical applications, while assuring accuracy and stability.

Keywords: hemorheology; shear thinning; blood viscosity; aggregation; Krieger model

1. Introduction

Mathematical simulations of blood flow require an appropriate constitutive model that accurately reflects its unique rheological properties, namely, shear thinning and the influence of hematocrit and plasma proteins. Several models of blood viscosity have been introduced over the past six decades, however most have focused on the shear thinning property (see Tables 1 and 2). Only a few models explicitly represent the mathematical dependence on hematocrit and protein concentrations. The latter property is important for simulating rheological anomalies that may occur in disease. The former property is important to account for the effect of hemodilution or hemo-concentration, as well as the non-uniform distribution of red blood cells in several situations, such as capillary tubes [1], plasma skimming [2], bifurcations [3], rotary blood pumps [4], and sudden expansions [5–7]. Several of the models presented in Tables 1 and 2 exhibit mathematical discontinuities with respect to shear rate and/or hematocrit. This study therefore investigates a quasi-mechanistic approach to explicitly account for a wide range of shear rate, hematocrit, and protein concentration to provide a convenient, rational viscosity model that is applicable to a broad range of conditions. The foundation of this work is the classical Krieger model for the viscosity of suspensions that accounts for volume fraction and the viscosity of the medium.

Table 1. Models of blood viscosity including a list of model features. X indicates the model has the feature and—indicates the model lacks the feature. (LS—low shear, HS—high shear).

Model	Equation	Shear Rate	Hematocrit	Proteins	Temperature	Asymptote LS/HS	Continuous	Legend
Newtonian [8]	$\eta = 0.0345\text{cP}$	–	–	–	–	–/X	X	(1)
Asymptotic [9]	$\eta = [\eta_0 + \eta_1\varphi - \eta_2\varphi^2 + \eta_3\varphi^3]P$	–	X	–	–	–/X	X	(2)
Power-Law [8]	$\eta = k\dot{\gamma}^{n-1}$	X	–	–	–	–/–	–	(3)
Generalized Power-Law [10]	$\eta = k(\dot{\gamma})\dot{\gamma}^{n(\dot{\gamma})-1}$	X	–	–	–	–/X	–	(4)
Walburn-Schneck (WS) [11]	$\eta = C_1\exp(C_2\varphi)\cdot\exp(C_4(TPMA/\varphi^2))\dot{\gamma}^{-C_3\varphi}$	X	X	X	X	–/–	–	(5)
Asymptotic Power-Law	$\eta = k\dot{\gamma}^{n-1} + \eta_\infty$	X	X	X	X	–/X	X	(6)
Cross, Modified Cross, Simplified Cross, Carreau, Carreau-Yasuda, Jung et al. [8,10,12,13]	$\eta = \eta_\infty + \Delta\eta\frac{1}{\left(1+(\lambda\dot{\gamma})^m\right)^a}$	X	–	–	–	X/X	X	(7)
Powell-Eyring [8]	$\eta = \eta_\infty + \Delta\eta\frac{\sinh^{-1}(\lambda\dot{\gamma})}{\lambda\dot{\gamma}}$	X	–	–	–	X/X	–	(8)
Modified Powell-Eyring [10]	$\eta = \eta_\infty + \Delta\eta\frac{\ln(1+\lambda\dot{\gamma})}{(\lambda\dot{\gamma})^m}$	X	–	–	–	X/X	–	(9)
Yeleswarapu [14]	$\eta = \eta_\infty + \Delta\eta\frac{1+\ln(1+\lambda\dot{\gamma})}{1+\lambda\dot{\gamma}}$	X	–	–	–	X/X	X	(10)
Quemada [15]	$\eta = \eta_{pl}(1 - 0.5K(\varphi,\dot{\gamma})\varphi)^{-2}$	X	X	–	–	–/X	–	(11)
Krieger [16]	$\eta = \eta_{pl}(1 - \frac{\varphi}{\varphi^*})^{-N}$	–	X	–	–	X/X	X	(12)

Table 2. Coefficients for blood viscosity models presented in Table 1.

Model	Coefficient Values	Ref.	Model	Coefficient Values	Ref.
Power-law	$k = 0.42$, $n = 0.61$	[8]	Walburn-Schneck (WS)	$C_1 = 0.00797$, $C_2 = 0.0608$, $C_3 = 0.00499$, $C_4 = 14.59$ L/g	[11]
Asymptotic	$\eta_0 = 0.014175$, $\eta_1 = 0.05878$, $\eta_2 = 0.1598$, $\eta_3 = 0.31964$	[9]	Modified Cross	$\eta_\infty = 3.5$ cP, $\Delta\eta = 52.5$ cP, $\lambda = 3.736$ s, $m = 2.406$, $a = 0.254$	[8]
Cross	$\eta_\infty = 3.5$ cP, $\Delta\eta = 52.5$ cP, $\lambda = 1.007$ s, $m = 1$, $a = 1.028$	[8]	Carreau-Yasuda	$\eta_\infty = 3.5$ cP, $\Delta\eta = 52.5$ cP, $\lambda = 1.902$ s, $m = 1.25$, $a = 0.7588$	[8]
Carreau	$\eta_\infty = 3.5$ cP, $\Delta\eta = 52.5$ cP, $\lambda = 3.313$ s, $m = 2$, $a = 0.3216$	[8]	Modified Power-Erying	$\eta_\infty = 3.5$ cP, $\Delta\eta = 52.5$ cP, $\lambda = 2.415$ s, $m = 1.089$	[10]
Powell-Erying	$\eta_\infty = 3.5$ cP, $\Delta\eta = 52.5$ cP, $\lambda = 5.383$ s	[8]	Yeleswarapu	$\eta_\infty = 5.0$ cP, $\Delta\eta = 68.6$ cP, $\lambda = 14.81$ s	[14]
Simplified Cross	$\eta_\infty = 5$ cP, $\Delta\eta = 125$ cP, $\lambda = 8.0$ s, $m = 1$, $a = 1$	[12]		–	

Table 2. *Cont.*

| Model	Coefficient Forms	Coefficients	Ref.
Generalized Power-Law	$k = \eta_\infty + \Delta\eta \exp(-\bar{\dot{\gamma}}_1 \exp(b/\dot{\gamma}))$ $n = 1 + \Delta n \exp(-\bar{\dot{\gamma}}_2 \exp(d/\dot{\gamma}))$	$\eta_\infty = 3.5$, $\Delta\eta = 25$, $\Delta n = 0.45$, $a = 50$, $b = 3$, $c = 50$, $d = 4$.	[10]
Jung et al. Modified Carreau	$a = (a_1\varphi + a_2\varphi^2 + a_3\varphi^3)k_o$ $\Delta\eta = \eta_{pl}(1 + d_1\varphi + d_2\varphi^2 + d_3\varphi^3)$ $k_o = 1 + Ko\left[\ln\left(\ln\left(1 + (\lambda\dot{\gamma})^2\right)\right)/\ln\left(1 + (\lambda\dot{\gamma})^2\right) - 1\right]$	$\eta_\infty = 0$, $\lambda = 0.1101$ s, $\dot{\gamma} \geq 6\,\text{s}^{-1}$ $Ko = 0$, $a_1 = 0.1752$, $a_2 = 0.4123$, $a_3 = -0.4046$, $d_1 = 16.305$, $d_2 = -51.213$, $d_3 = 122.28$, $\dot{\gamma} < 6\,\text{s}^{-1}$ $ko = 1$, $a_1 = 0.8907$, $a_2 = -1.0339$, $a_3 = -0.4456$, $d_1 = 9.7193$, $d_2 = -22.454$, $d_3 = 70.782$	[13]
Quemada Model (Cokelet)	$K = \dfrac{k_o + k_\infty\sqrt{\dot{\gamma}/\dot{\gamma}_c}}{1+\sqrt{\dot{\gamma}/\dot{\gamma}_c}}$ $k_o = \exp(a_o + a_1\varphi + a_2\varphi^2 + a_3\varphi^3)$ $k_\infty = \exp(b_o + b_1\varphi + b_2\varphi^2 + b_3\varphi^3)$ $\dot{\gamma}_c = \exp(c_o + c_1\varphi + c_2\varphi^2 + c_3\varphi^3)$	$a_o = 3.874$, $a_1 = -10.41$, $a_2 = 13.80$, $a_3 = -6.738$, $b_o = 1.3435$, $b_1 = -2.803$, $b_2 = 2.711$, $b_3 = -0.6479$, $c_o = -6.1508$, $c_1 = 27.923$, $c_2 = -25.60$, $c_3 = 3.697$	[17]
Quemada Model (Das)	As above, except: $k_o = a_0 + \dfrac{2}{a_1 + \varphi}$	as above, except: $a_o = 0.275363$ and $a_1 = 0.100158$	[18]

1.1. Factors that Contribute to the Viscosity of Blood

The apparent viscosity of whole blood, as measured using devices based on force or torque balance, may be altered by a variety of factors [19–21]. The most fundamental contributing factors are plasma viscosity [22], hematocrit, cell deformability [23–25], and aggregability [23]. Plasma viscosity is primarily affected by temperature [26] and the concentration of large molecules such as proteins, lipids, and polysaccharides [22,27]. Hematocrit can be altered by the hydration status of the individual [28], changes in the plasma osmotic pressure which affects the size of the red blood cells (RBCs) [29,30], the use of volume expanders [20], diseases like polycythemia [21] or anemias, and other conditions. The deformability of RBCs depends on their size and shape, membrane composition, cytoskeletal structure, temperature [19,26] (i.e., in the case of hypothermia), intracellular hemoglobin viscosity [31],

rate of erythropoiesis, and cell age [32]. RBC deformability may also be altered by previous cell trauma due to shear exposure [32]. RBC aggregation is affected by concentration of large proteins or macromolecules that can form links between the cells as well as by shear [22,23], cell size, shape, and deformability, pH [33], and plasma osmolality [34].

Several models have been proposed over the past six decades to account for the shear thinning behavior of blood. Table 1 provides a list of 13 popular models. (Their corresponding coefficients are provided in Table 2). These models treat blood as a single continuum in which shear thinning is represented by various regressions of apparent viscosity to experimental data, for example employing polynomial, exponential, logarithmic, and power law functions. The latter is one of the earliest and most commonly employed functions (see Equation (3)). However, it is only accurate over a limited range of shear rate, and therefore must be either re-fit piece-wise for different ranges of shear rate or the coefficients must be replaced by functions of shear rate (for example, Equation (5)). Subsequent models addressed this limitation by introducing a normalized shear thinning function that is scaled according to low-shear and asymptotic viscosities (see for example, Equations (7)–(10)). Various forms of a shear thinning functions have been proposed to improve the accuracy for the intermediate shear rates where the greatest transition occurs. More sophisticated models, such as the Walburn-Schneck (WS) model [11] (Equation (5)), explicitly account for the dependence of hematocrit, temperature, and protein concentration. However since it is also based on a power-law, it is subject to the associated limitations on shear rate, referenced above. The Quemada model [15] (Equation (11)), the Carreau-Yasuda (CY) model presented by Jung et al. [13] (Equation (7)), and the asymptotic viscosity model provided by Guyton [9] (Equation (2)) include hematocrit but not protein concentrations. The latter model also neglects shear thinning.

The Quemada model was shown to exhibit unbounded discontinuities at hematocrit values of 12.2%, 18%, 73.1%, and 85.6%. This is illustrated in Figure 1 for the baseline condition of zero shear rate. Das et al. [18] re-fit one of the coefficients, k_o (Hct), in an attempt to make the model continuous, yet a discontinuity still remains for zero shear rate at a hematocrit of 80.4%, which could be problematic for simulation of some pathological conditions such as polycythemia. The elevated viscosity due to the discontinuities at 12.2% and 18% are not as pronounced between shear rates of 1 s^{-1} to 10 s^{-1} (not shown in Figure 1), while the discontinuities at 73.1% and 85.6% persists up to 80 s^{-1}. The discontinuity found in the Das version persists well beyond 1000 s^{-1}; for example the viscosity at 150 s^{-1} is 7 times the experimental value. The modified CY model, such as used by Jung et al., [13] and the WS model both exhibit a discontinuity at zero shear rate and the WS model has also a discontinuity at zero hematocrit. Although infinite viscosity could be interpreted as a yield stress, this will prevent the convergence of most numerical schemes except in several simple cases.
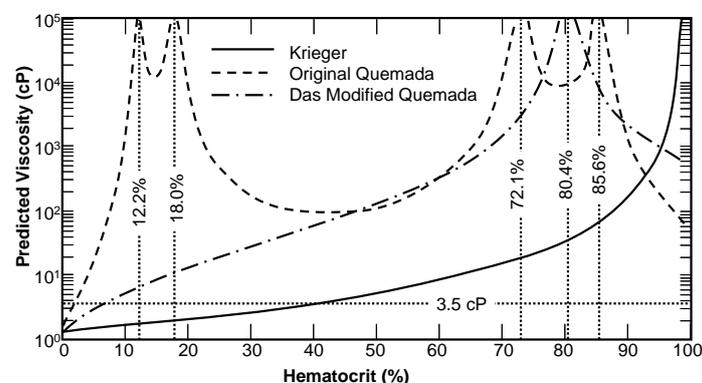
Figure 1. The zero-shear viscosity prediction of the original Quemada model, the modified Quemada model, and the Krieger model with *n* = 2. Discontinuities and regions where the viscosity is inversely proportional to hematocrit were found for both forms of the Quemada model.

In summary, a truly versatile model for blood viscosity should include functional dependence on shear rate, hematocrit, temperature, and plasma protein concentration, and should also be continuous over a wide range of these parameters. In addition, it is advantageous to construct a rational model starting from first principles that represent meaningful physical phenomena.

1.2. The Krieger Model of Viscosity of Suspensions

One viscosity model that satisfies the above requirements is the Krieger model, introduced in 1959, based on Eyring's *theory of rate processes* applied to suspensions of solid spheres [16]. One of its attractive features is the assumption that particles interact in a controlled manner over a finite time frame, which holds irrespective of their shape. However, since some of the mechanisms underlying the interaction of many types of particles are not mathematically characterized, this model has been empirically modified for specific applications, such as suspensions of irregularly shaped particles [35–38], deformable particles and emulsions [39,40], colloidal suspensions [41,42], and even blood [43,44].

2. Adaptation of the Krieger Viscosity Model for Blood

In this study, the Krieger model was modified to include the fundamental features of blood described above. Where possible, mechanistic relations were sought to minimize the need for empiricism. An additional goal was to avoid discontinuities and adverse extrapolative behavior. By replacing the particle concentration in the Krieger model with volume packing fraction, as described by Bowen [45], we can substitute hematocrit (Hct) into the equation. Likewise, the viscosity of the suspension medium becomes the plasma viscosity, η_{pl}. The resulting form of the Krieger model becomes:

$$\eta = \eta_{pl}\left(1 - \frac{\text{Hct}}{\text{Hct}^*}\right)^{-n} \quad (\text{Hct} \leq \text{Hct}^*) \tag{13}$$

where Hct* is the volume fraction at which the particles cease to flow, referred herein as the *critical hematocrit*. The exponent, *n* is a free model parameter, which in the classic Krieger formulation is a constant calculated from intrinsic viscosity and critical concentration. Theoretically, *n* is 1.66 for solid spheres, but empirically it has been shown to be closer to 2.0 [46]. To account for the unique properties of blood, this coefficient will be replaced below by a function of shear rate and hematocrit. Although Equation (13) no longer appears in the classic form, it is consistent with its later usage [36,47–49]. The three parameters of the Krieger model η_{pl}, Hct* and *n*, can be identified independently and are described in the following three sub-sections.

2.1. Plasma Viscosity

The plasma viscosity is primarily determined from the concentration of large molecules [LM] and temperature. Proteins, polysaccharides, and large lipids can all be considered large molecules, and so can additives such as Dextran commonly used to alter the shear stress when conducting experiments in vitro. Plasma viscosity can thus be expressed through linearization as:

$$\eta_{pl} = \bar{\eta}_{pl}\left(1 + \sum\left(\alpha_i([\text{LM}]_i - [\overline{\text{LM}}]_i)\right)\right) \tag{14}$$

where α is the proportionality constant (e.g., 2 cP/g% for fibrinogen [24]), and the bar indicates a reference value, assumed here to be the typical values for a normal, healthy individual. The units of LM can depend on the species, but are typically in g% or mg%. It should be cautioned that the linearization does not necessarily hold over a wide range. For example, a regression to the data of Wells et al. shows that α reduces to 0.51 cP/g% when the fibrinogen concentration reaches 2 g%.

The relationship for the temperature dependence of a viscous fluid is:

$$\ln \eta = a + b_t \ln T \tag{15}$$

which can be algebraically rearranged into the form:

$$\eta = \bar{\eta} \left(\frac{T}{\overline{\overline{T}}} \right)^{-b_t} \tag{16}$$

where T is the absolute temperature, a and b are material constants, and the bar again implies a reference value. This model is only valid for fluids within the neighborhood of the reference temperature. Based on regression to data from Snyder for plasma, the exponent, b_t was determined to be 5.95 for temperatures between 10 °C and 40 °C. The combination of Equations (14) and (16) yields a final expression for plasma viscosity:

$$\eta_{pl} = \bar{\eta}_{pl} \left(1 + \alpha([LM] - [\overline{LM}]) \right) \left(\frac{T}{\overline{\overline{T}}} \right)^{-b_t} \tag{17}$$

Normal plasma viscosity of a healthy individual has been reported within the range 1.10 cP to 1.35 cP. For the remainder of this study, a nominal value of 1.23 cP is used.

2.2. Critical Hematocrit

Hct* is the theoretical volume fraction at which red blood cells cease to behave as a fluid. This condition is equivalent to the mixture becoming a porous media which can sometimes behave as an elastic solid as well. Chien determined experimentally that blood concentrated to 98% Hct could continue to flow in a viscometer. It was however difficult to concentrate the blood further due to the limits of centrifugation. Therefore Hct* is believed to be in the range of 98% to 100% for normal blood. Using logical constraints on volume fraction, we therefore assumed Hct* to be 99% ± 1%. However, we acknowledge that decreased RBC deformability would reduce this value; in the extreme case of glutaraldehyde hardened cells, Hct* could be as low as 58%–60%. To assure that errors in specifying Hct* would not significantly alter the other parameter values, a sensitivity study for the best-fit model parameters was performed for a range of Hct* between 96% and 100%.

2.3. Krieger Exponent and Shear Thinning

The shear thinning aspect of blood is governed by disaggregation of RBCs at shear rates (above approximately $11 \, s^{-1}$) and the deformation of RBCs for moderate to high shear rates (between $10 \, s^{-1}$ and $150 \, s^{-1}$). Above this range, blood can be considered Newtonian. The aggregability of RBCs, in turn, is dependent on the concentration of plasma proteins, especially large molecules like fibrinogen and Dextran, the hematocrit, as well as the size, shape, and rigidity of RBCs [6,7,27]. The functional dependence of deformability includes the rigidity of the RBC as well as the hematocrit—since greater packing requires more net energy to deform the cells. In addition, the shear thinning behavior of blood only becomes significant above a specific hematocrit, therefore the Krieger exponent would lend itself to a piecewise definition:

$$n = n_\infty + \begin{cases} 0, & \text{Hct} < \text{Hct}^{st} \\ n_{st}, & \text{Hct} > \text{Hct}^{st} \end{cases} . \tag{18}$$

where $\overline{\overline{\text{Hct}}}$ is a threshold below which shear thinning is not observed, n_∞ contributes to the asymptotic viscosity and n_{st} refers to the shear thinning component. Rheometric data reported by Brooks et al. [50] exhibits negligible shear thinning for a hematocrit of 12.6% therefore $\overline{\overline{\text{Hct}}}$ was chosen conservatively to be 20%. Regression to these experimental data yielded an exponential dependence of n_∞ on Hct:

$$n_\infty = a + b \exp(-c \times \text{Hct}). \tag{19}$$

The exponent n_{st} was further decomposed into the respective contributions of RBC aggregation and deformability:

$$n_{st} = n_{agg} + n_{def} \tag{20}$$

Regression to the data of Brooks [50] showed that each of these components can be represented by power-law functions, therefore:

$$n_{st} = \beta_{agg}\gamma'^{-\nu_{agg}}_{agg} + \beta_{def}\gamma'^{-\nu_{def}}_{def} \tag{21}$$

where β and ν are empirical coefficients and γ' is a non-dimensional form of shear rate, introduced by Carreau and Yasuda [8]:

$$\gamma' = 1 + (\lambda\dot{\gamma})^{\nu_g}, \tag{22}$$

where λ is a proportionality constant having units of time and ν_g is traditionally 2.0. This form assures that n_{st} remains bounded at zero shear rate. Although an unbounded zero-shear viscosity has been proposed as a method for modeling yield stress, this discontinuity creates numerically instability and may be better represented through an explicit term in the constitutive law. Due to the limited size of the data set, it was more convenient to combine the components of shear thinning into a single power-law function [8]:

$$n_{st} = \beta\gamma'^{\nu}. \tag{23}$$

The dependence of β on fibrinogen concentration [*fg*] was represented based on steady states kinetics for saturating systems, constrained such that aggregation vanishes as [*fg*] approaches zero:

$$\beta_{agg} = B_1(1 - \exp(B_2[fg])), \tag{24}$$

where B_1 and B_2 are model constants. A Hill model would also be feasible for predicting saturation. The equation can be extrapolated to other molecules through addition of an identical term for each species considered.

3. Model Evaluation

3.1. Parameter Estimation

Two modified Krieger viscosity models were considered: (1) an asymptotic Krieger model (AKM) having 3 parameters with an asymptotic viscosity per Equation (19); and (2) a modified Krieger model having 5 parameters (MKM5) incorporating shear-thinning (i.e., combining Equations (18), (19), (22) and (23)) using constant values for β and ν. These models were fit to the viscosity data published by Brooks et al. [50] with seven values of hematocrit: 8.25%, 12.6%, 28.7%, 35.9%, 48%, 58.9%, and 67.4%, over a shear range of 0.4 s^{-1} to 700 s^{-1}. (Unless specifically noted, these data were used for all subsequent fits). ANOVA was used to determine the statistical significance and validity of each model constant and to ensure that each contributes to the model and is not simply an additional degree of freedom. These models were also compared with the Quemada model for a more qualitative assessment of fit and to demonstrate the relative order of the root mean square (RMS) error. The effect of hardening cells on the Krieger exponent n was investigated using data from Chien et al. [23] for hematocrits of 13%, 26%, 37%, 44%, 49%, 53%, and 56%. Additional coefficients, namely β_{agg}, ν_{agg}, β_{def}, ν_{def}, λ_{agg}, λ_{def}, B_1, and B_2, were found for the specific case of 45% hematocrit using additional data from Chien et al. using canine blood.

3.2. Sensitivity Study

A sensitivity study was performed on the viscosity models using fully-developed, steady-state Poiseuille flow with the Navier-Stokes equations for a generalized Newtonian fluid, wherein the governing equations simplify to:

$$\frac{\partial u_z}{\partial r} = \frac{1}{2}\frac{r}{\eta}\frac{dP}{dz},$$ (25)

with $u_z(r = R) = 0$ at the wall, assuming a no-slip condition and $u_r(r) = u_\theta(r) = 0$. The tube radius, *R*, was selected to be 0.6 cm. Flow was simulated at three different flow rates, 0.06 L/min, 0.6 L/min, and 6 L/min, equivalent to wall shear rates from approximately 6 s^{-1} to 600 s^{-1}. For the purpose of the sensitivity study, the Reynold's number was limited to the laminar regime (<2500), so that turbulence could be neglected. Equation (25) was numerically solved on a computer workstation using a first-order backwards-difference numerical scheme. The finite difference code was validated using the exact solutions to a Newtonian fluid and the power-law fluid. The solution was evaluated for four bulk hematocrits (20%, 40%, 60% and 75%), assuming a uniform Hct profile. An additional sensitivity study was performed assuming a parabolic hematocrit field:

$$\text{Hct}(z) = 2\overline{\text{Hct}}\left(1 - \left(\frac{r}{R}\right)^2\right),$$ (26)

where $\overline{\text{Hct}}$ is the bulk hematocrit, equivalent to the uniform cases. Three pressure gradients were prescribed to simulate two extreme conditions ($dp/dz = -1.0$ and -25 dyn/cm^3) and a nominal condition ($dp/dz = -10$). The velocity profile resulting from the modified Krieger, Quemada, and the modified Carreau models were compared for each case.

4. Results

Figure 2 compares the regressions of two Quemada models (QM) and the Krieger model (KM) to the viscosity data published by Brooks et al. [50]. Quemada model (QM), the Asymptotic Quemada model (QM, $k = k_\infty$), the constant-n Krieger model (KM) to the best-fit asymptotic Krieger model (AKM) (See Table 3 for parameters). The model with the worst fit to these data was the asymptotic Quemada model (RMS = 2.20 cP) followed by the Quemada model (RMS = 1.36 cP), and the Krieger model assuming $n = 2$, the value for solid spheres (RMS = 1.22 cP). The AKM showed a significant improvement ($p \ll 0.0001$) with the root mean square (RMS) of the residual = 0.212 cP and $R^2 = 0.99$. In addition, the 95% confidence intervals for the coefficients was less than 15%, indicating an overall goodness of fit and independence of coefficients. The AKM was least sensitive to the parameter *b*, as a 10% change in that parameter resulted in a 35% increase in the RMS value when compared to *a* and *c*, which resulted in a 376% and 200% changes respectively.
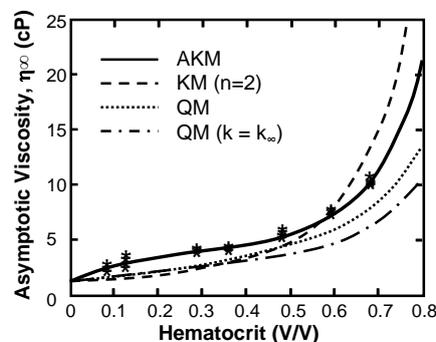

Figure 2. Comparison of regression of asymptotic viscosity vs. hematocrit with the Asymptotic Krieger model (AKM), Krieger model ($n = 2$), the Quemada model, and the asymptotic Quemada model ($k = k_\infty$) to the experimental data of Brooks et al. (asterisks) [49]. (Shear rate > 100 s^{-1}).

Table 3. The best fit parameters for the three modified Krieger models with 95% confidence intervals for the parameters as determined from Monte Carlo simulation.

Model Parameter	AKM	AKM (Fixed Cells)	MKM5	MKM9	Agg/Def. Model	*Fg* Model
a	1.70 (1.66–1.75)	1.06 (0.944–1.18)	0	0.686 (0.34–1.03)	0.0974	1.30
b	9.86 (8.63–11.1)	−0.226−(0.201–0.251)	8.71 (7.85–9.57)	11.8 (4.11–19.5)	n/a	n/a
c	6.07 (5.59–6.55)	−1.69−(1.54–1.85)	2.87 (2.55–3.20)	8.60 (3.42–13.8)	n/a	n/a
β	n/a	n/a	8.23 (7.85–8.60)	n/a	n/a	n/a
λ	n/a	n/a	108 (106–110)	136 (120–152)	n/a	n/a
ν	n/a	n/a	0.134 (0.122–0.146)	n/a	n/a	n/a
b_1	n/a	n/a	n/a	−9.11 −(10.7–7.48)	n/a	n/a
b_2	n/a	n/a	n/a	13.0 (12.2–13.9)	n/a	n/a
n_1	n/a	n/a	n/a	0.180 (0.090–0.269)	n/a	n/a
n_2	n/a	n/a	n/a	−0.170 −(0.304–0.035)	n/a	n/a
n_3	n/a	n/a	n/a	0.124 (0.073–0.174)	n/a	n/a
β_{agg}	n/a	n/a	n/a	n/a	4.27	n/a
λ_{agg}	n/a	n/a	n/a	n/a	24.1	16.0
ν_{agg}	n/a	n/a	n/a	n/a	0.380	0.0895
β_{def}	n/a	n/a	n/a	n/a	4.36	n/a
λ_{def}	n/a	n/a	n/a	n/a	5.44	n/a
ν_{def}	n/a	n/a	n/a	n/a	0.120	n/a
B_1	n/a	n/a	n/a	n/a	n/a	6.26
B_2	n/a	n/a	n/a	n/a	n/a	5.54

The AKM coefficients were also fit to data for rigid cells (e.g., hardened by glutaraldehyde) and resulted in an RMS of 10.7 cP and an R^2 value of 0.997 (See Table 3). All three coefficients were altered: a was reduced by 29%, b was reduced by almost an order of magnitude, and c changed in sign causing N to increase exponentially. The optimal critical hematocrit was 58.5% ± 0.8% which agrees well with the value predicted by Carr and Cokelet [24]. It was also found that the AKM model for the hardened cells showed significant ($p < 0.0005$) improvement vs. the constant-n model, confirmed by the corrected Akaike information criterion δAICc = −50.0.

Figure 3 provides the fit of apparent viscosity over four decades of shear rate (0–1000 s^{-1}) for the MKM5 to the experimental data of Brooks et al. [49] with constant β and ν. It was found that the parameter a (Equation (19)) was not significantly different from 0 ($p = 0.17$) and was therefore removed from the model, reducing the number of free parameters to five. It was also shown that ν_g did not vary significantly from the commonly used value of 2 ($p = 0.79$; δAICc = 3.7). The RMS error was 1.74 cP with an R^2 value > 0.98. The maximum absolute error occurred at the shear rates of 1 s^{-1} and Hct of 67.4%, while the maximum percent error occurred at a shear rate of 17 s^{-1} and a Hct of 8.25%. The 95% confidence intervals for the model parameters were 11.3% for the parameter c. The 5-parameter modified Krieger model MKM5 was least sensitive to λ, as a 10% change in λ resulted in only a 19.5% increase in the RMS value, while similar deviations resulted in changes greater than 80%. The modified Krieger model showed similar accuracy as the Quemada model, despite fewer parameters (RMS error = 1.74 vs. 4.07). Both models showed similar accuracy for low hematocrit (<25%). The modified Krieger model showed better overall fit for moderate hematocrit values when compared to the Quemada model, with the opposite trend for high hematocrit (>55%). The R^2 value for the Quemada model was 0.914. The initial form of the MKM5 allowed the shear-thinning behavior due to aggregability to be treated independently from the effect of cell deformation. This is illustrated in Figure 4 which shows the viscosity function consisting of Equations (18)–(22). The values for β were within 3% when comparing aggregation to deformation; but the values for relaxation time (λ) and the exponent (ν) differed by factors of 5 and 4 respectively. The relationship of fibrinogen and the low shear viscosity is illustrated in Figure 5. The optimal values for parameters B_1 and B_2 are provided in Table 3.
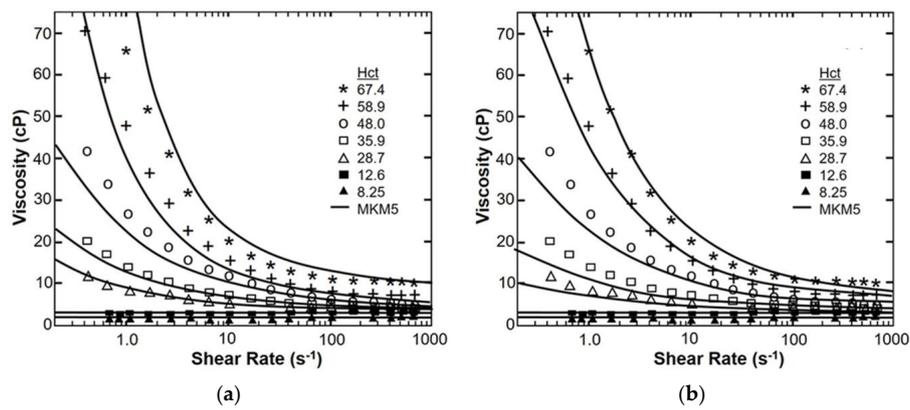
Figure 3. A comparison of shear thinning according to the MKM5 (**a**) and the Quemada model (**b**) vs. the experimental data of Brooks et al. [49] (symbols) for seven values of hematocrit and spanning four decades of shear rate.
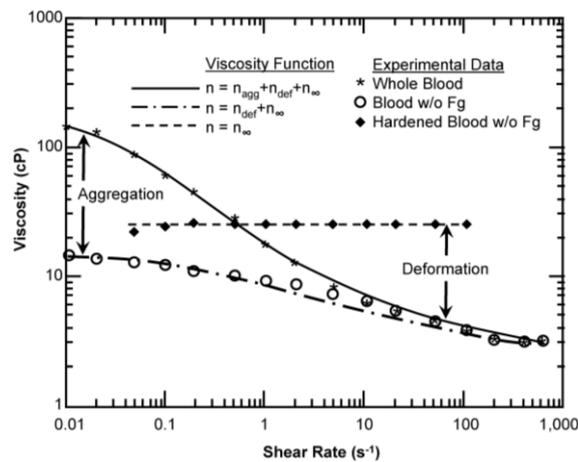

Figure 4. Contribution of aggregation and cell deformation on viscosity for canine red blood cells (RBCs) at a hematocrit of 45% and a temperature of 37 °C. The lines for each case are generated from the modified Krieger model with the appropriate optimal parameters. Experimental data from Chien [50].
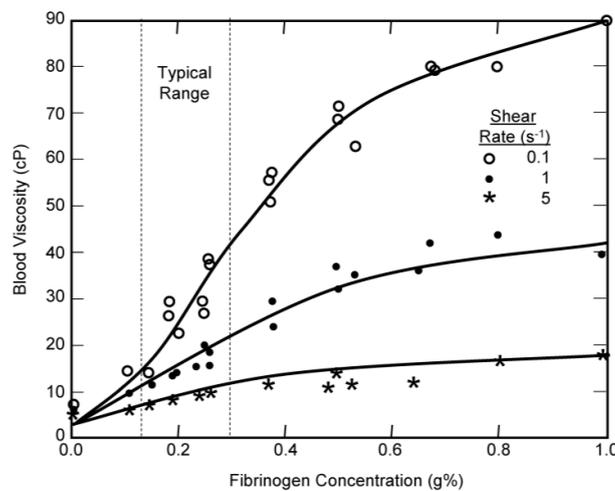

Figure 5. The effect of fibrinogen concentration on the viscosity of 45% canine blood at a temperature of 37 °C. Comparison of experimental data from Chien [23] with the modified Krieger model.

Sensitivity Study of Shear Thinning Behavior in Tube Flow

The solution for fully-developed flow in a tube having a radius of 0.6 cm, using a hematocrit of 40%, for the three pressure gradients studied resulted in flow rates of 0.06, 0.6, and 6.0 L/min. The mesh spacing was approximately 1.4 pm (pico meters), corresponding to approximately 500×10^6 elements. All three results exhibited the expected velocity blunting phenomenon, which was considerably more pronounced at low flow rate (Figure 6a) compared to high flow rate (Figure 6b.) Irrespective of the flow rate, the MKM5 and Quemada models were very similar, with a maximum difference of centerline velocity less than 1%. The modified Cross model (used by Jung) showed more blunting than both the modified Krieger (MKM5) and Quemada models for all three conditions. Similar results were found when varying the bulk hematocrit, but differences were found to be greater (maximum differences 4%). The introduction of a parabolic hematocrit profile to each of the three models demonstrated a more pronounced blunting effect on the velocity profile (see Figure 7). For the high-flow case (not shown) the centerline velocity was reduced by 36% compared to the Newtonian profile, and 25% compared to the MKM5 shear-thinning model with uniform Hct.
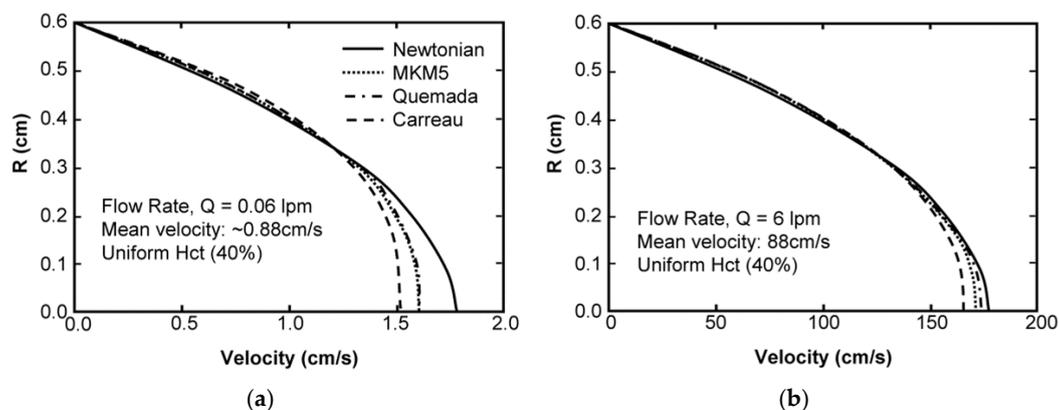
Figure 6. The fully-developed, steady-state velocity profile for Poiseuille flow of 40% hematocrit blood in a tube. Results compare the Newtonian solution (Parabolic), with the Modified Krieger model, the modified Quemada Model, and the model used by Jung et al. at a flow rate of 0.06 lpm (**a**) and 6 lpm (**b**).
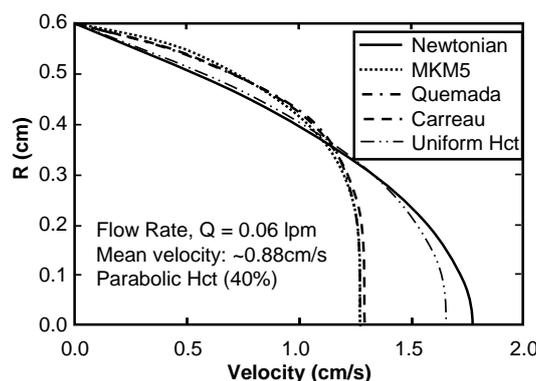
Figure 7. Comparison of the fully-developed, steady-state velocity profile for Poiseuille flow of blood assuming a parabolic hematocrit profile vs. a uniform profile. The results of the MKM5 model and Quemada model overlap.

5. Discussion

Increasing reliance is being given to numerical simulation in the development of medical devices and evaluation of vascular diseases. Consequently, the accuracy of blood flow simulations has

undergone increased scrutiny. Most simulations are performed using an asymptotic viscosity for blood (approximately 3.5 cP), based on the assumption that shear rates are sufficiently great to neglect shear thinning, and thereby allowing the use of the Navier-Stokes equations. Although asymptotic viscosity is acceptable for evaluating flows in simple geometries under certain circumstances, errors of up to 18% have been reported in complex geometries that feature regions of recirculation and/or pulsatility. Figure 6 shows that even at very high shear rates ($>$500 s^{-1}) velocity profile blunting due to shear thinning is still observable in tube flow. The consequence of these errors propagates into the calculation of derived quantities of interest, such as shear stress, hemolysis, and transport of leukocytes, platelets, and various chemical species. Moreover, the asymptotic blood viscosity is not a universal constant. It depends on several blood parameters (hematocrit, plasma viscosity, and RBC deformability) that vary from person to person. Micro-scale flow, such as in micro-fluidic devices or small arterioles may introduce inhomogeneity of hematocrit (e.g., due to plasma skimming), and therefore in these situations it is advantageous to employ a hematocrit-dependent formula for viscosity. Recent interest in pediatric medical devices, cryogenic surgery, the use of drag reducing polymers, plasma dilution, and other areas of study can also benefit from a viscosity model of blood that can accommodate localized variations in hematocrit, temperature, and/or protein concentration.

The Krieger model of viscosity of particulate solutions was used as the basis for the present model, and was modified to account for shear thinning, hematocrit dependence, and other influences on the viscosity of blood, including temperature, fibrinogen concentration, and red blood cell deformability. This approach strikes a balance between a purely empirical regression to data vs. a micro-mechanistic model that accounts for fluid-solid interactions and collisions between cells. Although Krieger derived his model based on the assumption of rigid spheres, its fundamental premise is Eyring's theory of rate processes which is valid for any particles that interact with each other in a finite manner. Therefore, it is reasonable to believe that the Krieger model should still reliably hold for blood, albeit with a different exponent. Because the Krieger model is based on well-established theory of particulate suspensions, it has an additional advantage over empirical models is that extrapolation outside the experimental range of the data poses less risk of error—such as the discontinuities exhibited by the other models in Figure 1.

A 5-parameter modified Krieger model, MKM5, showed a similar RMS accuracy when compared to the viscosity model of Quemada despite requiring 7 fewer parameters. The MKM5 also demonstrated improved accuracy over the physiological range of hematocrits (30%–50%) when compared to the Quemada model (It is worth noting the Quemada model was also the assumption of a particulate solution). Simulations of blood flow in a tube using the MKM5 model exhibited anticipated behavior: velocity profile blunting at low shear rates that became less pronounced at higher shear rates. The shear thinning behavior likewise increased with increasing hematocrit.

The effect of inhomogeneity of hematocrit is often neglected when simulating blood flow. The potential for error was illustrated in this study in Figure 7 for the case of blood flow in a tube. This prompts caution when simulating flow in vessels or channels of small diameter, as well as disturbed flow, small gaps such as the occluder of a prosthetic valve, or blade tips of a rotodynamic blood pump [4], and even Couette devices . In the current study, the hematocrit profiles were explicitly prescribed. In practice, they could be supplied directly from experimental measurements or from computations using a multi-phase constitutive model of blood.

Although the current model includes explicit functional dependence on several of the most relevant variables used in blood rheology (hematocrit, plasma protein concentration, temperature, and shear rate), additional functional dependence could potentially be introduced to make it more versatile. For example, the shear thinning coefficients β and ν could be replaced by functions that are explicitly dependent on hematocrit, such as the following Taylor expansions:

$$\beta(\text{Hct}) = b_1 \text{Hct} + b_2 \tag{27}$$

and

$$\nu(\text{Hct}) = n_1\text{Hct}^2 + n_2\text{Hct} + n_3 \tag{28}$$

where b_1, b_2, n_1, n_2, n_3 are empirical constants. This would result in a 9-parameter modified Krieger model (MKM9). Yet additional coefficients would be needed to explicitly include the influence of red blood cell deformability on high-shear viscosity and aggregability on low-shear viscosity. Although these effects are non-negligible, they would require a rather extensive set of experiments, in the manner described by Chien et al. [23], to identify the functional relationships. These properties are also inter-dependent, since RBC aggregation is affected by RBC deformability and shape, as well as the concentration of fibrinogen and other large molecules. RBC shape, in turn, could include functional dependence on the osmolarity of plasma (or suspension medium in vitro) and temperature. In summary, the number of parameters needed to account for all known dependencies and inter-dependencies can quickly become unwieldy with respect to the quantity of experimental data needed to identify them uniquely, and avoid over-fitting. Therefore, it is logical to limit the complexity of the model to those factors that are relevant for a given application.

It is also important to realize that the addition of independent variables may lead to a completely different set of coefficients. For example, a regression of the high-shear, asymptotic viscosity of blood n_∞ to the associated asymptotic data (Figure 2) yielded a different set of parameters ($a = 1.7$, $c = 6.06$) than when the full model was fit to the full set of data (Figure 3), ($a = 0.0$, $c = 2.87$.) This is also illustrated for Equation (7) in Table 1 where a single equation represents six different models with drastically different parameters (Table 3).

Conversely, the use of reduced order, simplified models may have an advantage of more determinate coefficients. However, such models should be used with caution: considering the relevance of their assumptions to the problem at hand, as well as constraints affecting their accuracy. For example, in the Krieger models presented here, the aggregability and deformability were prescribed for a single hematocrit (Figure 4), hence coefficients b and c could not be uniquely determined. Another example is the effect of fibrinogen on aggregation as shown in Figure 5. This case was limited to the range of shear rate of $0.1\,\text{s}^{-1}$ to $5\,\text{s}^{-1}$, compared to the data sets shown in Figures 2 and 3 where the maximum shear rate was two orders greater. This demonstrates both the limitations of the model, and a call for a richer set of experimental data. Future work should also include validation beyond the simple viscometric flows that were used to calibrate the model. By considering a diversity of practical applications, it would elucidate anomalies introduced by an overly-simplified viscosity model and how they can be corrected by quasi-mechanistic models, such as those presented here.

6. Conclusions

Mathematical models of blood rheology span a broad spectrum of complexity. Increasing complexity provides benefits in some situations but brings additional costs. The commonly used Newtonian model, employing an asymptotic viscosity, offers computational efficiency and may be perfectly adequate for large scale problems with sufficiently high shear stress. On the other hand, simulations in which the shear rate and/or hematocrit is spatially heterogeneous might demand a more sophisticated model that explicitly accounts for their influence on viscosity. In addition, in states of disease such as diabetes, polycythemia, and cardiovascular disease, additional considerations should be made for abnormalities in blood rheology. The use of medical devices, such as hemodialysis, cardiopulmonary bypass, etc. are also known to alter the mechanical properties of blood. The Krieger models presented here can be considered a practical compromise between a purely empirical fit to data and a fully detailed mechanistic model for situations in which variations in hematocrit, protein concentration, and shear rate are non-negligible.

References

1. Fahraeus, R.; Lindvist, T. The viscosity of the blood in narrow capillary tubes. *Am. J. Physiol. Leg. Content* **1931**, *96*, 562–568.

2. Palmer, A.A. Axial drift of cells and partial plasma skimming in blood flowing through glass slits. *Am. J. Physiol. Leg. Content* **1965**, *209*, 1115–1122.

3. Cho, Y.I.; Kensey, K.R. Effects of the non-Newtonian viscosity of blood on flows in a diseased arterial vessel. Part 1: Steady flows. *Biorheology* **1991**, *28*, 241–262. [PubMed]

4. Kim, N.J.; Diao, C.; Ahn, K.H.; Lee, S.J.; Kameneva, M.V.; Antaki, J.F. Parametric study of blade tip clearance, flow rate, and impeller speed on blood damage in rotary blood pump. *Artif. Organs* **2009**, *33*, 468–474. [CrossRef] [PubMed]

5. Karino, T.; Goldsmith, H.L. Flow behaviour of blood cells and rigid spheres in an annular vortex. *Philos. Trans. R. Soc. Lond. B Biol. Sci.* **1977**, *279*, 413–445. [CrossRef] [PubMed]

6. Wootton, D.M.; Markou, C.P.; Hanson, S.R.; Ku, D.N. A mechanistic model of acute platelet accumulation in thrombogenic stenoses. *Ann. Biomed. Eng.* **2001**, *29*, 321–329. [CrossRef] [PubMed]

7. Zhao, R.; Marhefka, J.N.; Shu, F.; Hund, S.J.; Kameneva, M.V.; Antaki, J.F. Micro-flow visualization of red blood cell-enhanced platelet concentration at sudden expansion. *Ann. Biomed. Eng.* **2008**, *36*, 1130–1141. [CrossRef] [PubMed]

8. Sequeira, A.; Janela, J. An Overview of Some Mathematical Models of Blood Rheology. In *A Portrait of State-of-the-Art Research at the Technical University of Lisbon*; Pereira, M.S., Ed.; Springer: Lisbon, Portugal, 2007; pp. 65–87.

9. Guyton, A.C. *Textbook of Medical Physiology*; Saunders: Philadelphia, PA, USA, 1981.

10. Ballyk, P.D.; Steinman, D.A.; Ethier, C.R. Simulation of non-Newtonian blood flow in an end-to-side anastomosis. *Biorheology* **1994**, *31*, 565–586. [PubMed]

11. Walburn, F.J.; Schneck, D.J. A constitutive equation for whole human blood. *Biorheology* **1976**, *13*, 201–210. [PubMed]

12. Steffan, H.; Brandstätter, W.; Bachler, G.; Pucher, R. Comparison of Newtonian and Non-Newtonian Blood Flow in Stenotic Vessels using Numerical Simulation. In *Biofluid Mechanics*; Springer: Berlin, Heidelberg, 1990; pp. 479–485.

13. Jung, J.; Hassanein, A. Three-phase CFD analytical modeling of blood flow. *Med. Eng. Phys.* **2008**, *30*, 91–103. [CrossRef] [PubMed]

14. Yeleswarapu, K.K.; Kameneva, M.V.; Rajagopal, K.R.; Antaki, J.F. The flow of blood in tubes: Theory and experiment. *Mech. Res. Commun.* **1998**, *25*, 257–262. [CrossRef]

15. Quemada, D. Rheology of Concentrated Disperse Systems. II. Model for Non-Newtonian Shear Viscosity in Steady Flows. *Rheol. Acta* **1978**, *17*, 632–642. [CrossRef]

16. Krieger, I.M.; Dougherty, T.J. A mechanism for non-Newtonian flow in suspensions of rigid spheres. *Trans. Soc. Rheol.* **1959**, *3*, 137–152. [CrossRef]

17. Cokelet, G.R.; Brown, J.R.; Codd, S.L.; Seymour, J.D. Magnetic resonance microscopy determined velocity and hematocrit distrubutions in a Couette viscometer. *Biorheology* **2005**, *42*, 385–399. [PubMed]

18. Das, B.; Johnson, P.C.; Popel, A.S. Effect of nonaxisymmetric hematocrit distribution on non-Newtonian blood flow in small tubes. *Biorheology* **1998**, *35*, 69–87. [CrossRef]

19. Kameneva, M.V.; Ündar, A.; Antaki, J.F.; Watach, M.J.; Calhoon, J.H.; Borovetz, H.S. Decrease in red blood cell deformability caused by hypothermia, hemodilution, and mechanical stress: Factors related to cardiopulmonary bypass. *ASAIO J.* **1999**, *45*, 307–310. [CrossRef] [PubMed]

20. Eckmann, D.M.; Bowers, S.; Stecker, M.; Cheung, A.T. Hematocrit, volume expander, temperature, and shear rate effects on blood viscosity. *Anesth. Analg.* **2000**, *91*, 539–545. [CrossRef] [PubMed]

21. Rosenkrantz, T.S. Polycythemia and hyperviscosity in the newborn. *Semin. Thromb. Hemost.* **2003**, *29*, 515–528. [PubMed]

22. Rand, P.; Barker, N.; Lacombe, E. Effects of plasma viscosity and aggregation on whole-blood viscosity. *Am. J. Physiol. Leg. Content* **1970**, *218*, 681–688.

23. Chien, S.; Usami, S.; Dellenback, R.J.; Gregersen, M.I.; Nanninga, L.B.; Guest, M.M. Blood viscosity: Influence of erythrocyte deformation. *Science* **1967**, *157*, 827–829. [CrossRef] [PubMed]

24. Carr, R.; Cockelet, G.R. Rheology of suspensions of normal and hardened erythrocytes and their mixtures. *J. Rheol.* **1981**, *25*, 67–82. [CrossRef]

25. Baskurtand, O.K.; Meiselman, H.J. Cellular determinants of low-shear blood viscosity. *Biorheology* **1997**, *34*, 235–247. [CrossRef]

26. Snyder, G. Influence of temperature and hematocrit on blood viscosity. *Am. J. Physiol. Leg. Content* **1971**, *220*, 1667–1672.

27. Chien, S.; Usami, S.; Taylor, H.M.; Lundberg, J.L.; Gregersen, M.I. Effects of hematocrit and plasma proteins on human blood rheology at low shear rates. *J. Appl. Physiol.* **1966**, *21*, 81–87. [PubMed]

28. Armstrong, L.E. Hydration assessment techniques. *Nutr. Rev.* **2005**, *63*, S40–S54. [CrossRef] [PubMed]

29. Rand, P.W.; Lacombe, E. Hemodilution, tonicity, and blood viscosity. *J. Clin. Investig.* **1964**, *43*, 2214–2226. [CrossRef] [PubMed]

30. Sidel, V.W.; Solomon, A.K. Entrance of water into human red cells under an osmotic pressure gradient. *J. Gen. Physiol.* **1957**, *41*, 243–257. [CrossRef] [PubMed]

31. Herrmann, A.; Müller, P. Correlation of the internal microviscosity of human erythrocytes to the cell volume and the viscosity of hemoglobin solutions. *Biochim. Biophys. Acta Mol. Cell Res.* **1986**, *885*, 80–87. [CrossRef]

32. Kameneva, M.V.; Antaki, J.F.; Borovetz, H.S.; Griffith, B.P.; Butler, K.C.; Yeleswarapu, K.K.; Watach, M.J.; Kormos, R.L. Mechanisms of red blood cell trauma in assisted circulation: Rheologic similarities of red blood cell transformations due to natural aging and mechanical stress. *Asaio J.* **1995**, *41*, M457–M460. [CrossRef] [PubMed]

33. Rand, P.W.; Austin, W.H.; Lacombe, E.; Barker, N. pH and blood viscosity. *J. Appl. Physiol.* **1968**, *25*, 550–559. [PubMed]

34. Reinhart, W.H.; Piety, N.Z.; Goede, J.S.; Shevkoplyas, S.S. Effect of osmolality on erythrocyte rheology and perfusion of an artificial microvascular network. *Microvasc. Res.* **2015**, *98*, 102–107. [CrossRef] [PubMed]

35. Keller, D.S.; Keller, D.V. The effect of particle size distribution on the antithixotropic and shear thickening properties of coal-water dispersions. *J. Rheol.* **1991**, *35*, 1583–1607. [CrossRef]

36. Allende, M.; Kaylon, D.M. Assessment of particle-migration effects in pressure-driven viscometric flow. *J. Rheol.* **2000**, *44*, 79–89. [CrossRef]

37. Huang, N.; Bonn, D. Viscosity of a dense suspension in Couette flow. *J. Fluid Mech.* **2007**, *590*, 497–507. [CrossRef]

38. Jogun, S.; Zukoski, C.F. Rheology of dense suspensions of platelike particles. *J. Rheol.* **1996**, *40*, 1211–1232. [CrossRef]

39. Bullard, J.W.; Pauli, A.T.; Garboczi, E.J.; Martys, N.S. A comparison of viscosity-concentration relationships for emulsions. *J. Colloid Interface Sci.* **2009**, *330*, 186–193. [CrossRef] [PubMed]

40. Niedzwiedz, K.; Buggisch, H.; Willenbacher, N. Extensional rheology of concentrated emulsions as probed by capillary breakup elongational rheometry (CaBER). *Rheol. Acta* **2010**, *49*, 1103–1116. [CrossRef]

41. Lionberger, R.A. Shear thinning of colloidal dispersions. *J. Rheol.* **1998**, *42*, 843–863. [CrossRef]

42. Heyes, D.M.; Sigurgeirsson, H. The Newtonian viscosity of concentrated stabilized dispersions: Comparisons with the hard sphere fluid. *J. Rheol.* **2004**, *48*, 223–248. [CrossRef]

43. Mansour, M.H.; Bressloff, N.W.; Shearman, C.P. Red blood cell migration in microvessels. *Biorheology* **2010**, *47*, 73–93. [PubMed]

44. Pal, R. Rheology of concentrated suspensions of deformable elastic particles such as human erythrocytes. *J. Biomech.* **2003**, *36*, 981–989. [CrossRef]

45. Bowen, R.M. Theory of mixtures. In *Continuum Physics III*; Erningen, A.C., Ed.; Academic Press: New York, NY, USA, 1976; pp. 1–127.

46. Ovarlez, G.; Bertrand, F.; Rodts, S. Local determination of the constitutive law of a dense suspension of noncolloidal particles through magnetic resonance imaging. *J. Rheol.* **2006**, *50*, 259–292. [CrossRef]

47. Aidun, C.K.; Clausen, J.R. Lattice-Boltzmann method for complex flows. *Annu. Rev. Fluid Mech.* **2010**, *42*, 439–472. [CrossRef]

48. Fradette, L.; Tanguy, P.A.; Bertrand, F.; Thibault, F.; Ritz, J.-B.; Giraud, E. CFD phenomenological model of solid–liquid mixing in stirred vessels. *Comput. Chem. Eng.* **2007**, *31*, 334–345. [CrossRef]
49. Frith, W.J.; d'Haene, P.; Buscall, R.; Mewis, J. Shear thickening in model suspensions of sterically stabilized particles. *J. Rheol.* **1996**, *40*, 531–548. [CrossRef]
50. Brooks, D.E.; Goodwin, J.W.; Seaman, G.V. Interactions among erythrocytes under shear. *J. Appl. Physiol.* **1970**, *28*, 172–177. [PubMed]